Cite this : New Carbon Materials, 2023, 38(5): 964-975 **DOI:** 10.1016/S1872-5805(23)60707-3

Synthesis and electrochemical properties of nano-Si/C composite anodes for lithium-ion batteries

YUAN Li-ye[1,2,*], LU Chun-xiang[1,2,*], LU Xiao-xuan[1,2], YUAN Shu-xia[1,2], ZHANG Meng[1,2,3], CAO Li-juan[1,2], YANG Yu[1,2]

（1. *National Engineering Laboratory for Carbon Fiber Technology*, *Institute of Coal Chemistry*, *Chinese Academy of Sciences*, *Taiyuan* 030001, *China*;
2. *CAS Key Laboratory of Carbon Materials*, *Institute of Coal Chemistry*, *Chinese Academy of Sciences*, *Taiyuan* 030001, *China*;
3. *University of Chinese Academy of Sciences*, *Beijing* 100049, *China*）

Abstract: Phenolic resin was coated on the surface of nano-Si by a microencapsulation technique, and then carbonized under Ar protection to prepare a nano-Si/C composite. The composites were first prepared using 4 different mass ratios (1∶2, 1∶4, 1∶6, 1∶8) of phenolic resin to nano-Si. The obtained average thicknesses of amorphous carbon coating were 7, 4.5, 3.7, 2.8 nm, respectively. By comparing the cycling and rate capability, the best electrochemical performance was obtained when this ratio was 1∶4, with a 4.5 nm amorphous carbon coating. The electrochemical properties of this material were then comprehensively evaluated, showing excellent electrochemical performance as an anode material for Li-ion batteries. At a current density of 100 mAg^{-1}, the material had a first specific discharge capacity of 2 382 $mAhg^{-1}$, a first charge specific capacity of 1 667 $mAhg^{-1}$, and an initial coulombic efficiency of 70%. A discharge specific capacity of 835.6 $mAhg^{-1}$ was retained after 200 cycles with a high coulombic efficiency of 99.2%. In addition, the nano-Si/C composite demonstrated superior rate performance. Under current densities of 100, 200, 500, 1 000 and 2 000 mAg^{-1}, the average specific discharge capacities were 1 716.4, 1 231.6, 911.7, 676.1 and 339.8 mAh g^{-1}, respectively. When the current density returned to 100 mA g^{-1}, the specific capacity returned to 1 326.4 mAh g^{-1}.

Key words: Microencapsulation technology; Lithium-ion batteries; Silicon anode; High capacity; Low-cost

1 Introduction

Lithium-ion batteries (LIBs) have been widely used in portable electronic products and electric vehicles[1], attributing to their high energy density, operating voltage, low self-discharge characteristics and maintenance requirements[2]. Currently, graphite is the most widely used anode material for commercial LIBs because of their excellent electronic conductivity, high coulombic efficiency and low charge-discharge electrochemical over-potential[3]. However, its theoretical specific capacity is only 372 mAh g, which hardly meets the increasing requirement of anode materials for high-capacity and high-power LIBs[4]. Owning to high theoretical specific capacity (3 579 mAh g^{-1}), low discharge platform (~ 0.45 V *vs*. Li/Li^+), limited reactivity with electrolytes, abundant earth reserves and environmental friendliness, silicon (Si) is one of the most promising candidates that could replace graphite as the next-generation anode material for LIBs[5–7]. However, silicon-based anode materials also have serious disadvantages. For example, considerable volume change is usually accompanied with the charging and discharging process. This huge volume variation could lead to the pulverization and shedding of silicon particles and the rupture of electrode coating, resulting in rapid capacity attenuation and poor cyclic stability[8–13].

In order to overcome the above shortcomings, a number of methods have been proposed to optimize the Si-based anodes. One typical method is designing nanoscale silicon materials, such as silicon nanoparticles, silicon nanofibers and silicon nanotubes. In this way, the absolute volume change of silicon particles could be reduced during the charge and discharge process, alleviating the induced stress from volume expansion[14–20]. Moreover, the nanoscale anode materials could also significantly increase the sur-

Received date: 2020-09-10; **Revised date:** 2020-10-29

Corresponding author: YUAN Li-ye, Assistant research fellow. E-mail: cimigowatano@163.com;
LU Chun-xiang, Professor. E-mail: lucx@sxicc.ac.cn

face area and grain boundary of silicon anodes, which can effectively shorten the diffusion path of lithium ions, and promote the rapid formation of silicon-lithium compounds from lithium ions with silicon[21]. Another classic approach to restrain the capacity attenuation of silicon anodes is to coat a carbon layer on the surface of silicon nanoparticles to build a silicon/carbon (Si/C) nanocomposite[22–26]. During the charge-discharge process, the outer carbon coating would not merely act as a buffer layer to limit the volume expansion of silicon nanoparticles[27–29], but also prevent the reaction between silicon nanoparticles and electrolyte. Therefore, nano-Si/C nanocomposite is considered as one of the most promising anode materials for high-capacity and high-power lithium-ion batteries[30].

At present, numerous methods have been reported to prepare nano-Si/C nanocomposites, such as mixing the nano-Si with graphite[31–33], combining nano-Si with various carbon precursors[34–37], and combining graphite, carbon precursors with nano-Si[38–39]. In this paper, a fast, efficient and cost-effective method is reported to synthesize a new nano-Si/C nanocomposite with superior electrochemical performance. Briefly, quantitative phenolic resin was first coated on the nano-Si evenly as carbon precursor *via* microcapsule technology. The obtained core-shell structure was then calcinated in the argon atmosphere to prepare nano-Si/C nanocomposite anode material. Benefiting from the hard carbon gained by carbonizing phenolic resin, the electrical conductivity of nanocomposite was significantly improved, leading to the enhanced electrical contact of electrode. More importantly, the volume change of nano-Si could be alleviated attributing to the mechanical strength of hard carbon. The electron microscopy characterization showed that the surface of nano-Si is uniformly coated with hard carbon, while the electrochemical tests of the prepared nano-Si/C nanocomposite anode material demonstrated that its discharging specific capacity could reach as high as 2 382 mAh g^{-1}, and after 100 cycles, 1 035 mAh g^{-1} capacity could be retained. Moreover, the nano-Si/C anode also exhibited excellent rate performance.

2 Experimental

2.1 Materials

Commercial nano-Si was purchased from Shanghai McLean Biochemical Technology Co. Ltd. (100 nm, 99%). Phenolic resin was obtained from Shandong Balun New Material Technology Co. Ltd. Silicon oil was purchased from Dow Corning Co. Ltd. (AR). Ethyl alcohol was purchased from Tianjin Tianli Chemical Reagent Co., Ltd. (AR). Carbon tetrachloride was purchased from Tianjin FengChuan chemical reagent Technology Co., Ltd. (AR). All the chemical reagents were directly used without any special handling.

2.2 Material characterization

The morphologies as well as particle size of nano-Si/C nanocomposite were observed by the field emission electron microscopy (FE-SEM, JSM-7900F) and transmission electron microscopy (TEM, JEM-2100F). The crystalline structure was determined by X-ray diffraction (XRD, D8 ADVANCE A25) and micro-Raman spectroscopy (Raman, HR800-632.8). The thermal decomposition of the nano-Si/C nanocomposite was studied by thermal gravimetric analyzer (TG, TGA 2) from 60 to 700 °C at 10 °C/min under the airflow.

2.3 Electrochemistry characterization

The working electrode was prepared by mixing the nano-Si/C nanocomposite as active material, carbon black as conductive additive with PVDF as the binder at the ratio of 8∶1∶1, using NMP as the solvent. The above mixture slurry was casted at a thickness of 100 μm and pressed on copper foil as the current collector. The collector was then dried at 80 °C under vacuum for 24 h. The prepared collector worked as working electrode and pure lithium metal used as reference electrode were assembled as CR2032-type cells in an Ar-filled glovebox. Celgard2500 polyethylene was used as the separator. Commercial electrolyte of 1 mol L^{-1} $LiPF_6$ dissolved in a mixture of ethylene carbonate (EC), dimethyl carbonate (DMC), diethyl carbonate (DEC) with a ratio of 1∶1∶1, and 5% fluoroethylene carbonate (FEC)

was added as additives. Galvanostatic charge and discharge (GCD) cycling and rate performance were measured in a voltage range from 0.01 to 3.0 V by LANDCT 2001A battery test system. Cyclic voltammetry (CV) was measured using an electrochemical workstation (Chenhua, CHI 660E) at a scanning rate of 0.1 mV s^{-1}. Electrochemical impedance spectroscopy (EIS) tests were performed within the frequency range of 100 kHz to 0.01 Hz with an AC-amplitude of 10 mV.

3 Results and discussion

Fig. 1 schematically illustrates the synthesis process of nano-Si/C nanocomposite. Firstly, phenolic resin was dissolved in ethyl alcohol to form a transparent solution, and the concentration of the phenolic resin solution was 1%. Nano-Si which was 4 times the mass of phenolic resin was then dispersed in the solution (Fig. 1a). The dispersion was added into the silicon oil which worked as continuous phase, and the whole system was stirred to form a stable emulsion (Fig. 1b). Next, the emulsion was heated to cure phenolic resin (Fig. 1c). The nano-Si microcapsules coated with phenolic resin were obtained after being filtered, washed and dried in vacuum (Fig. 1d). Finally, the nano-Si microcapsules were carbonized in a tube furnace under an argon atmosphere to obtain an even coating of hard carbon on nano-Si particles, denoted as nano-Si/C nanocomposite (Fig. 1e).

Fig. 2a shows the Raman spectroscopy analysis of nano-Si/C nanocomposite and nano-Si as reference sample. The nano-Si showed 3 peaks at low frequency (i.e., 297, 507 and 927 cm^{-1}) that are derived from silicon lattice stretching. For nano-Si/C nanocomposite, the same 3 low frequency peaks could be identified, indicating the crystal structure of nano Si was preserved. Moreover, two other high frequency peaks (i.e., 1 362 and 1 594 cm^{-1}) could also be observed. These two peaks originated from the characteristic *D* (disordered) and *G* (graphitic) peaks of carbon materials. The relatively higher *D*/*G* ratio indicate the existence of amorphous carbon in nano-Si/C. Fig. 2b shows the X-ray diffraction patterns of nano-Si and nano-Si/C nanocomposite. Both of the patterns exhibited the same sharp diffraction peaks of crystal silicon, corresponding to the lattice plane of (111), (220), (311), (400) and (331), respectively. This consistence of silicon pattern demonstrates that the crystal silicon was not oxidized to SiO_x during the preparation. Moreover, a broad band at 20°-27° could be ob-

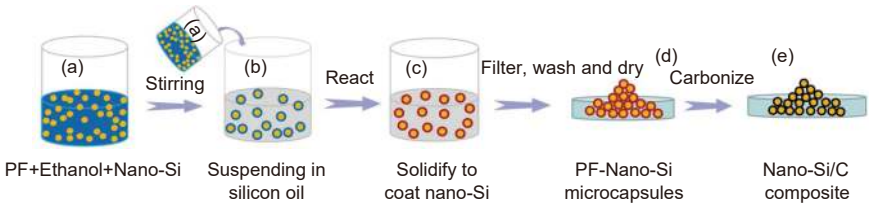

Fig. 1 Schematic illustration of synthesis of nano-Si/C nanocomposite

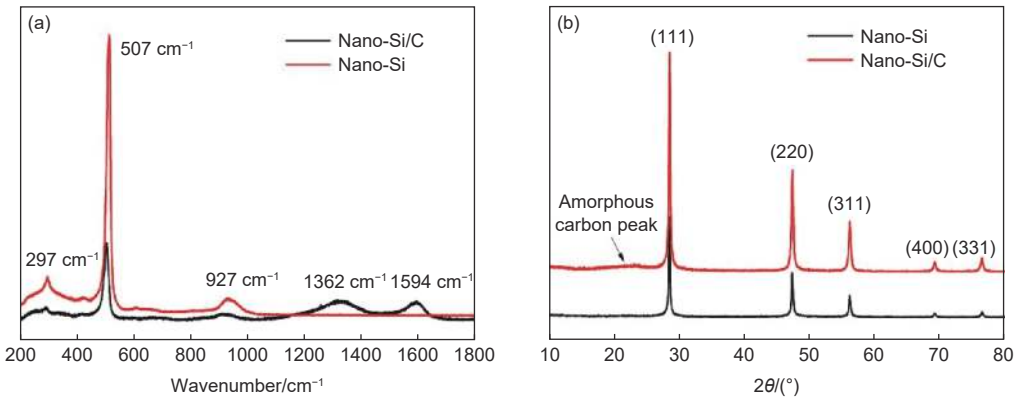

Fig. 2 (a) Raman and (b) XRD spectra of nano-Si and nano-Si/C samples

served at low intensity from nano-Si/C, which could be attributed to the amorphous carbon from the carbonization of resin, implying the the existence of carbon coating in the nano-Si/C nanocomposite.

Fig. 3 shows the SEM images of nano-Si and nano-Si/C nanocomposite. It could be observed that both the nano-Si and nano-Si/C nanocomposite presented spherical shape (Fig. 3a-b). Nano-Si/C nanocomposite exhibited rough surface, owing to the carbon coating around the surface of nano-Si particles.

Transmission electron microscopy (TEM) and corresponding high-resolution transmission electron microscopy (HRTEM) images of nano-Si/C are shown in Fig. 4. Clearly, all the nano-Si particles were encapsulated by a carbon coating (Fig. 4a, c) 4.5 nm in thickness. As shown in Fig. 4d, the well-ordered lattice spacing of 0.316 nm corresponds to the (111) plane of cubic Si, demonstrating that crystal silicon was not oxidized to SiO_x. The SAED image of nano-Si/C in Fig. 4b demonstrates that the nano-Si in nano-Si/C nanocomposite retained a spherical monocrystalline structure.

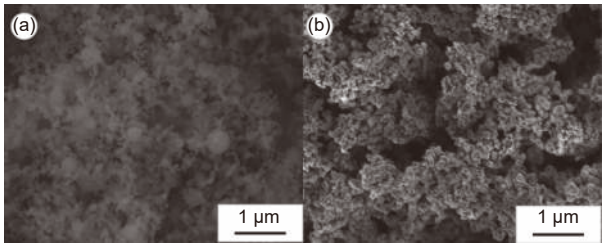

Fig. 3　Scanning electron microscopy (SEM) images of (a) nano-Si and (b) nano-Si/C

In order to investigate the influence of carbon coating thickness on the electrochemical performance of nano-Si/C nanocomposite, four different mass ratios of phenolic resin and nano-Si (1 ∶ 2, 1 ∶ 4, 1 ∶ 6 and 1 ∶ 8) were employed (Fig. 5). As shown in the TEM images, when the mass ratio of phenolic resin to nano-Si was 1 ∶ 2, 1 ∶ 4, 1 ∶ 6 and 1 ∶ 8, the average thickness of amorphous carbon coating was 7 (Fig. 5a), 4.5 (Fig. 5b), 3.7 (Fig. 5c) and 2.8 nm (Fig. 5d), respectively. This thickness variation suggests that a smaller ratio of phenolic resin to nano-Si results in thinner carbon coating.

Thermogravimetric analysis was performed on amorphous carbon obtained by direct carbonization of phenolic resin, nano-Si, and nano-Si/C nanocomposite prepared by 4 different mass ratios of phenolic resin to nano-Si (Fig. 6). The temperature range was 60-700 °C, and the heating rate was 10 °C min^{-1}. The analysis revealed that a significant weight loss of 93% for amorphous carbon was observed at high temperature, attributed to the oxidation of carbon to CO_2 in the air flow. Comparatively, the weight of nano-Si slightly increased about 1.63%, owning to the forma-

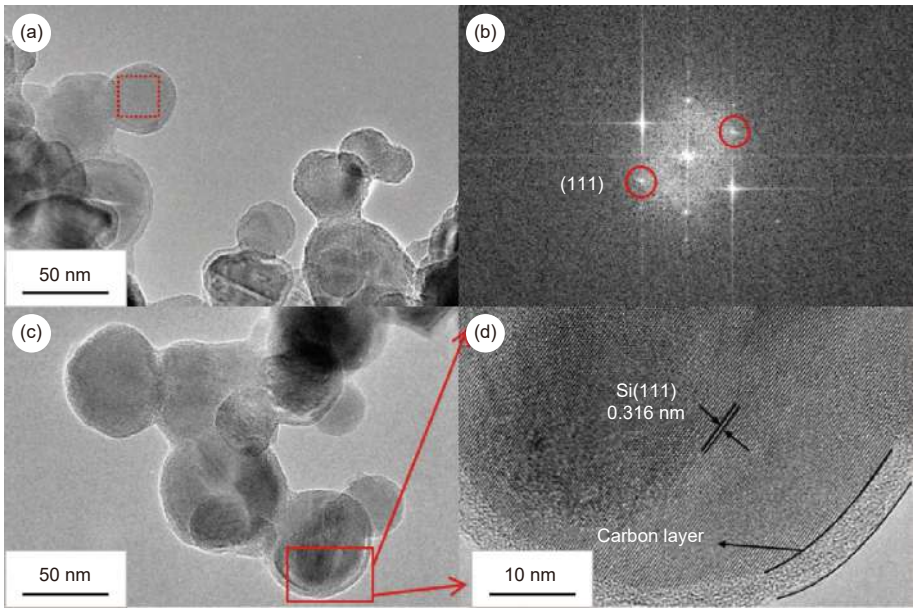

Fig. 4　(a, c) TEM images of nano-Si/C; (b) SAED image for the region highlighted by red square in (a); (d) HRTEM image of nano-Si/C

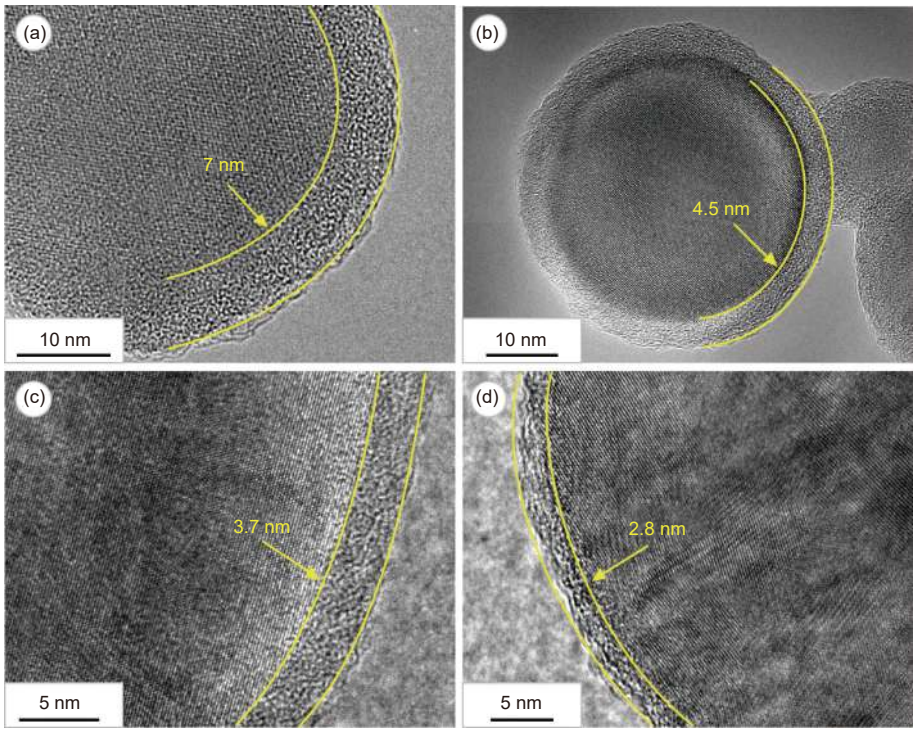

Fig. 5 TEM of nano-Si/C composite obtained by different mass ratios of phenolic resin to nano-Si: (a) 1∶2, (b) 1∶4, (c) 1∶6 and (d) 1∶8

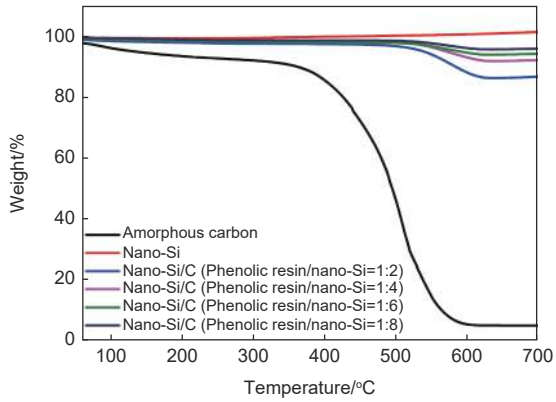

Fig. 6 Thermogravimetric analysis of amorphous carbon, nano-Si and nano-Si/C nanocomposites obtained by different mass ratios of phenolic resin to nano-Si

tion of a silica layer under oxidative atmosphere. The weight losses of nano-Si/C nanocomposites were 12.27%, 7.31%, 5.16% and 3.80%, corresponding to different mass ratios of phenolic resin to nano-Si, 1∶2, 1∶4, 1∶6 and 1∶8, respectively. Therefore, the weight loss of nano-Si/C nanocomposite could mainly be attributed to the oxidation of surface amorphous carbon coating. Moreover, it is shown that with the decrease of thickness of carbon coating, the weight loss also decreased accordingly.

Fig. 7a shows the cycling performance of four nano-Si/C nanocomposites obtained by different mass ratios of phenolic resin to nano-Si. When the ratio was 1∶2, the first charging specific capacity was 1 317.2 mAh g^{-1} at the current density of 100 mA g^{-1}. After 50 cycles, the capacity retention was about 352.2 mAh g^{-1}. For the ratio of 1∶4, the first charging specific capacity was 1 667 mAh g^{-1}, after 50 cycles of charging and discharging process, the remaining specific capacity was 1 253.7 mAh g^{-1}. When the ratio was increased to 1∶6, the first charge specific capacity of prepared nano-Si/C nanocomposite was 1 232.2 mAh g^{-1}. And the charging specific capacity retained of 947.4 mAh g^{-1} after 50 cycles. When the ratio was 1∶8 for nano-Si/C nanocomposite, the first charge specific capacity and the reserved specific capacity after 50 cycles were 1 117 and 626.3 mAh g^{-1}, respectively. As shown in Fig. 5, the thickness of amorphous carbon coating was 7.5, 4.5, 3.7 and 2.8 nm, respectively, corresponding to different mass ratios of phenolic resin to nano-Si. When the carbon coating was extremely thin, its mechanical strength was too weak to sustain the swelling of nano-Si dur-

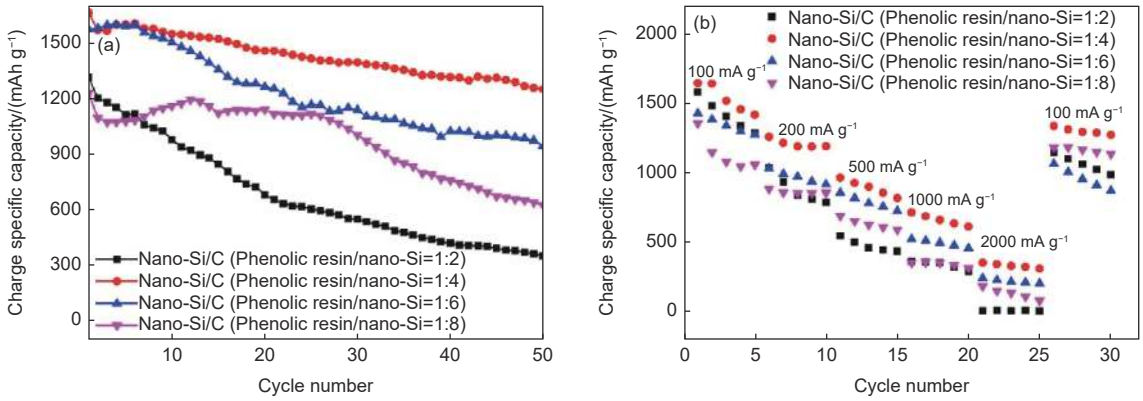

Fig. 7　Comparison diagrams of electrochemical performance of nano-Si/C nanocomposites obtained by different mass ratios of phenolic resin to nano-Si and (a) cycle performance and (b) rate performance

ing the charging and discharging process. With the increase of cycles, the carbon coating would suffer fatigue damage, and fall off from the inner silicon particle. Upon collapse, this carbon coating loses its protective effects, thus compromising the cycling performance. However, when the carbon coating was too thick, it would also negatively impact the cycling performance. This could be explained by considering that with the increase of carbon coating thickness, the migration channel of lithium ions became longer, making the insertion and extraction of lithium ions to silicon anode much difficult. Some lithium ions would also block the channel and turned into dead lithium, resulting in reduced capacity and poor cycling performance. According to the cycling results, the optimal mass ratio of phenolic resin to nano-Si was determined as 1∶4, and the corresponding carbon coating thickness was 4.5 nm.

Fig. 7b shows the rate performance of nano-Si/C nanocomposite obtained by different mass ratios of phenolic resin to nano-Si. For ratio of 1∶2, the average specific capacity of nano-Si/C nanocomposite was 1 420.1 mAh g^{-1} at the current density of 100 mA g^{-1}. While at current density of 200, 500, 1 000 and 2 000 mA g^{-1}, the average specific capacities were 882.48, 478.52, 337.3, and 8.1 mAh g^{-1}, respectively. When the current density returned to 100 mA g^{-1}, the specific capacity could be restored to 1 064.5 mAh g^{-1}. For ratio of 1∶4, at the current density of 100, 200, 500, 1 000 and 2 000 mA g^{-1}, the average specific capacity were 1 536.9, 1 209.7, 893.8, 663.2 and 332.6 mAh g^{-1}, respectively. When the current density returned to 100 mA g^{-1}, the specific capacity could be restored to 1 301.6 mAh g^{-1}. When the ratio was 1∶6, the average specific capacity of nano-Si/C nanocomposite was 1 346.1, 971.7, 788.9, 494, 221.1 and 962.8 mAh g^{-1} at current density of 100, 200, 500, 1 000, 2 000 and 100 mA g^{-1}, respectively. However, when the ratio was 1∶8, the average specific capacity of nano-Si/C nanocomposite was 1 137.7, 861.6, 634.7, 343.8, 132.7 and 1 164.4 mAh g^{-1}, respectively. It is shown that nano-Si/C nanocomposite at phenolic resin to nano-Si ratio of 1∶4 exhibited the highest specific capacity at both large and small current density. The excellent reversibility of the capacity could be attributed to the much improved electrical conductivity, with enhanced electric polarization reaction of nano-Si and its maximized utilization during the cycling process, leading to the higher specific capacity in the large current density. Moreover, the good mechanical properties of carbon coating could restrain the expansion of nano-Si, protecting the structural integrity of nano-Si, so the specific capacity of nano-Si/C nanocomposite could be restored to a higher level. However, as mentioned above, when the carbon coating was too thick, the lithium ions migration channel became longer. The electric polarization reaction was sped up when the current density was increased, congesting the ions migration channel and leading to a sharp drop in specific capacity. Therefore, 4.5 nm carbon coating obtained from phenolic resin to nano-Si ratio of 1∶4 was the optimal thickness for

nano-Si/C nanocomposite.

In order to observe the surface morphology changes of active substances after charge and discharge cycles, the nano-Si and 4 different electrodes mentioned above after 50 cycles were observed by FE-SEM. As shown in Fig. 8a, spherical nano-Si particles are barely visible since the structure undergoes pulverization and disintegration after the charge and discharge cycles. Fig. 8b-e are the morphology images of nano-Si/C electrodes after cycles, whose mass ratios of phenolic resin to nano-Si are 1∶2, 1∶4, 1∶6 and 1∶8, respectively. When the mass ratio is 1∶2 and 1∶4 (Fig. 8b-c), the thicknesses of carbon coating are larger in this 4 kinds of electrodes, therefore their mechanical strengths are high enough to effectively confine the volume expansion of nano-Si particles in the cycling process, helping them retain a good spherical shape. In Fig. 8d, cracks and pulverization begin to appear on the surface of the electrode, it is due to the smaller thickness of amorphous carbon coating which does not have a mechanical strength strong enough to withstand the volume expansion of nano-Si particles inside. With the decrease in mass ratio of phenolic resin to nano-Si, cracks and pulverization become more serious (Fig. 8e).

The following measurements were further employed on the optimal nano-Si/C nanocomposite (carbon coating of 4.5 nm) to comprehensively evaluate its electrochemical performance. Fig. 9a shows the charge and discharge curves of nano-Si/C nanocomposite at 1st, 2nd, 50th, 100th and 200th cycles, respectively. The discharge curve had a long plateau below 0.1 V, corresponding to the alloying process of crystalline silicon and lithium. The inclined voltage platform on the charge curve corresponded to the lithium escaping process to form amorphous silicon. The initial discharge specific capacity was 2 383 mAh g^{-1}, and the first coulombic efficiency was 70%. This efficiency loss was mainly due to the decomposition of electrolyte to form SEI membrane during the first charge and discharge process. The 2nd, 50th, 100th and 200th discharge specific capacity was 1 932, 1 227.4, 1 035 and 835.6 mAh g^{-1} respectively. Moreover, a stable charging plateau at 0.5 V could be observed from the first to the 200th cycle, indicating the excellent cycling performance of nano-Si/C anode composite.

Fig. 9b shows the cyclic voltammetry (CV) curves of nano-Si/C nanocomposite after different cycles. The CV curves were measured by the half-cell test at a voltage of 0.05-1.5 V and a sweep rate of 0.1 mV s^{-1}. In the first cycle, a reduction peak appeared during the cathode scanning around 0.67 V, corresponding to the decomposition of electrolyte and

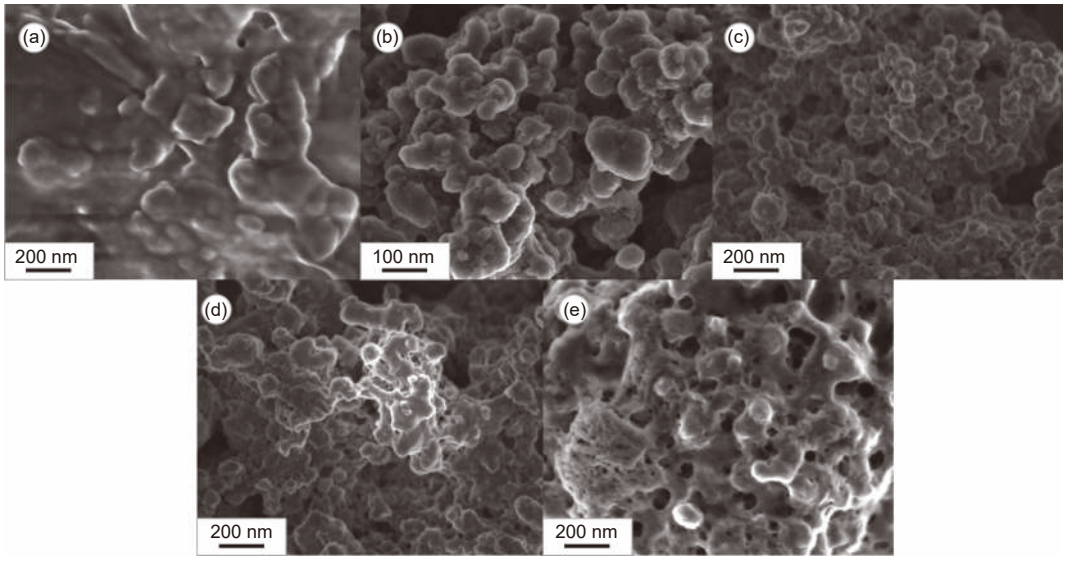

Fig. 8 FE-SEM images of nano-Si and the different nano-Si/C electrodes after 50 cycles: (a) nano-Si electrode, (b-e) nano-Si/C electrodes (Phenolic resin/nano-Si=1∶2, 1∶4, 1∶6 and 1∶8, respectively)

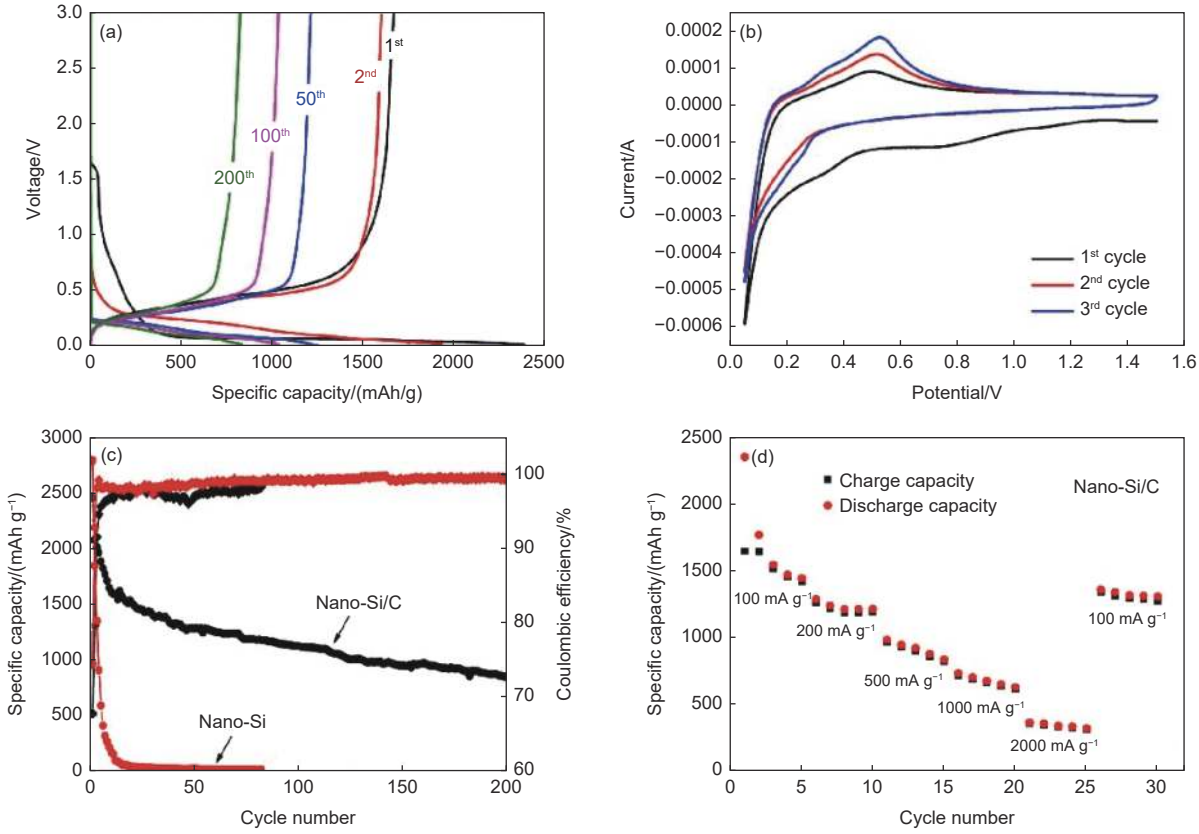

Fig. 9　Electrochemical performance of nano-Si/C electrode with an amorphous carbon coating thickness of 4.5 nm: (a) the discharge and charge curves, (b) cycle voltammetry measurements, (c) cycling property at 100 mA g^{-1} and coulombic efficiency of nano-Si/C nanocomposite, (d) the high-rate cycling performance of nano-Si/C electrode

the formation of SEI. It disappeared in the subsequent scanning process, indicating the formation of stable SEI during the 1st cycle. The cathode peak at 0.2 V was ascribed to the amorphization of crystalline silicon for lithiation[40–44]. During the first anodic scanning, the oxidation peak at 0.33 and 0.52 V corresponded to the phase transition reaction from amorphous Li_xSi to amorphous Si[45–46].

Fig. 9c shows the cycling performance of nano-Si/C nanocomposite. It is well known that pure nano-Si has a high first reversible specific capacity (2 793 mAh g^{-1}), but declines rapidly. After 80 cycles, only 8.4 mAh g^{-1} specific capacity could be retained. However, the core-shell structural nano-Si/C nanocomposite featuring pyrolyzed carbon coating exhibited excellent cycling stability. At 100 mA g^{-1}, the first discharge specific capacity is 2 383 mAh g^{-1}, the charging specific capacity was 1 667 mAh g^{-1}, and the first coulombic efficiency was 70%, with the capacity retention as high as 835.6 mAh g^{-1} after 200 cycles. Moreover, during the cycling process, the coulombic efficiency could be maintained above 94%, demonstrating its outstanding cycling stability. This boost to stability could be attributed to the unique core-shell structure of nano-Si/C naocomposite and carbon coating, which buffered the volume expansion of active silicon during the cycling process and maintained the electrical contact within the battery.

In Table 1 some recent works on Si-based composites as anodes for LIBs are quantified. Du et al.[47] prepared a novel Si-based composites (Si@C-AL-azo-NO_2) which exhibited a high reversible specific capacity of 882 mAh g^{-1} at a current density of 200 mA g^{-1} over 150 cycles and an initial coulombic efficiency (CE) of 65%. Chen et al.[48] synthesized a new nanofiber of silicon/carbon with hollow core-shell structure, whose reversible capacity was 1 020.7 mAh g^{-1} after 100 cycles at 0.2 A g^{-1} and initial CE was 53.4%. Fang et al.[49] prepared a unique core-shell structure of silicon@titania (Si@TiO_2) composites, which had a

Table 1 Comparison of the recent work on Si-based composites as anodes for Lithium-ion batteries

Samples	Current density/A g^{-1}	Cycle number	Capacity/mAh g^{-1} after cycles	Initial CE/%	References
Si@C-AL-zao-NO_2	0.20	150	882	65.0	[47]
Si@HC/CNF	0.20	100	1021	53.4	[48]
Si@TiO_2	0.42	100	804	51.3	[49]
HSi@C	0.50	200	886	52.4	[50]
Si-PBI	1.00	200	1128	60.3	[51]
nc-Si@HCS	0.25	250	810	69.0	[52]
Nano-Si/C	0.10	200	835	70.0	This work

high capacity of 804 mAh g^{-1} and a initial CE of 51.3% after 100 cycles at 0.1 C. It is evident that the initial CE of the nano-Si/C nanocomposite in this work is better than most of the previously reported results, while the cycling stability and capacity retention of nano-Si/C nanocomposite are apparently not so high. For the nanocomposite prepared with 1∶4, the capacity is 1 667 mAh g^{-1} at the current density of 100 mA g^{-1}, and reaches a value of 1 253 and 834.6 mAh g^{-1} after 50 and 200 cycles, respectively. In the first 50 cycles, the attenuation rate of single cycle is 0.49%, while in the following 150 cycles, it decrease to 0.22%. It demonstrates the structure of nano-Si/C nanocomposite become increasingly stable and the capacity attenuation tends to flatten out. There is room for improving the capacity retention of nano-Si@C nanocomposite with further research.

Fig. 9d shows the rate performance of optimal nano-Si/C nanocomposite. Under the current density of 100 mA g^{-1}, the average specific capacity of nano-Si/C was 1 716.4 mAh g^{-1}. While at the current densities of 200, 500, 1 000 and 2 000 mA g^{-1}, the average specific capacities were 1 231.6, 911.7, 676.1 and 339.8 mAh g^{-1}, respectively. When the current density returned to 100 mA g^{-1}, the specific capacity was restored to 1 326.4 mAh g^{-1}. Comparatively, the average specific capacities of bare nano-Si were about 2 300, 700, 250, 40 mAh g^{-1} at current densities of 100, 500, 1 000, 2 000 mA g^{-1}. When the current density returned to 100 mA g^{-1}, only 1 000 mAh g^{-1} specific capacity could be restored[53]. This excellent reversibility demonstrates that the core-shell structure was beneficial for the transportation of Li^+ and electrons, thus suggesting that carbon coating could significantly improve the conductivity of the silicon material.

Fig. 10 shows the electrochemical impedance spectra (EIS) of nano-Si and nano-Si/C electrodes. As shown in Fig. 9, the EIS curves were fitted by an equivalent circuit model, where R_s, CPE, R_1 (R_r) and W_1 represent Ohmic impedance, double-layer capacitance, charge transfer impedance and Warburg impedance tail, respectively. The electrochemical impedance spectra were composed of a semicircle in the high frequency region, a semicircle in the intermediate frequency region and an inclined line in the low frequency region. The semicircle in the high frequency region corresponded to the interface impedance of electrolyte and electrode surface, namely the SEI film impedance. The semicircle of the intermediate frequency region corresponded to the charge transfer impedance of lithium-ion embedded active substance. The inclined line in the low frequency region corresponded to the diffusion impedance of the ions in the electrode. It was found that for nano-Si/C electrode the semicircle radius in the high frequency was much smaller than that of nano-Si electrode, which proved that the core-shell structure of nano-Si/C and carbon coating could significantly facilitate the charge

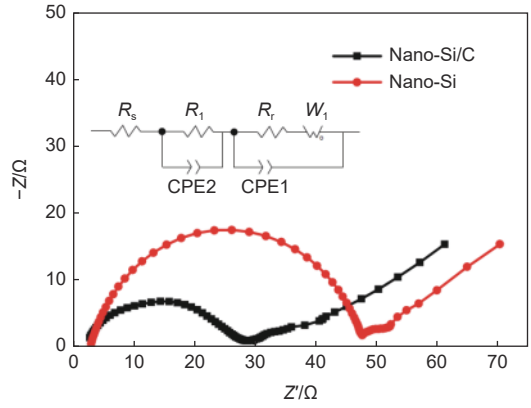

Fig. 10 Nyquist plots of nano-Si and nano-Si/C electrodes

transfer process, provide effective ion transfer path, and generate uniform SEI film on the electrode particles. Therefore, the SEI film impedance and the charge transfer impedance were reduced in the battery.

4 Conclusion

In summary, phenolic resin was coated on the surface of nano-Si particles *via in-situ* polymerization using a microencapsulation technique. The nano-Si/C nanocomposite was then obtained by carbonization under the Ar atmosphere. The nano-Si/C nanocomposite presented a core-shell structure, featuring nano-Si inner core and amorphous carbon coating with controllable thickness. When the mass ratio of phenolic resin to nano-Si was 1∶4, the prepared nano-Si/C nanocomposite exhibited the best electrochemical properties, and its outer carbon coating had an uniform thickness of 4.5 nm. The optimized carbon coating would not only effectively alleviate the volume expansion of nano-Si during the cycling process, but also improve the conductivity of the anode material. The lithium-ion battery electrode prepared by the nanocomposite demonstrated excellent cycling stability. At the current density of 100 mA g^{-1}, the specific capacity is 835.6 mAh g^{-1} after 200 cycles with a high coulombic efficiency (99.2%). Moreover, the superior rate performance is also promising for application in LIBs. Therefore, the reported novel core-shell structural nano-Si/C *via* microencapsulation technique could provide a new simple, efficient and cost-effective pathway for providing environmentally friendly anode materials.

Data availability statement

The data that support the findings of this study are openly available in Science Data Bank at https://cstr.cn/31253.11.sciencedb.09527 or https://doi.org/10.57760/sciencedb.09527.

Acknowledgements

This work is funded by “Supported by Fundamental Research Program of Shanxi Province (20210302124312)”. We would also like to thank Shiyanjia Lab (www.shiyanjia.com) for the XRD analysis.

References

[1] Huang X, Meng J, Liu W, et al. Lithium-ion battery lifetime extension with positive pulsed current charging[J]. Ieee Transactions on Industrial Electronics, 2024, 71(1): 484-635.

[2] Jin X, Han Y, Zhang Z, et al. Mesoporous Single-crystal lithium titanate enabling fast-charging li-ion batteries[J]. Advanced Materials, 2022, 34(210935618)

[3] Liu W P, Xu H R, Qin H Q, et al. The effect of carbon coating on graphite@nano-Si composite as anode materials for Li-ion batteries[J]. Journal of Solid State Electrochemistry, 2019, 23: 3363-3372.

[4] Wang M Y, Yin L, Li M Q, et al. Low-cost heterogeneous dual-carbon shells coated silicon monoxide porous composites as anodes for high-performance lithium-ion batteries[J]. Journal of Colloid and Interface Science, 2019, 549: 225-235.

[5] Liangruksa M, Kanaphan Y, Meethong N, et al. First-principles investigation of defective graphene anchored with small silicon clusters as a potential anode material for lithium-ion batteries[J]. Surface Science. 2023, 737(122250).

[6] Li P, Miao C, Yi D, et al. Pomegranate like silicon-carbon composites prepared from lignin-derived phenolic resins as anode materials for lithium-ion batteries[J]. New Journal of Chemistry, 2023

[7] Dong Q C, Yang J, Wu M Y, et al. Template-free synthesis of cobalt silicate nanoparticles decorated nanosheets for high performance lithium-ion batteries[J]. ACS Sustain Chemistry & Engineering, 2018, 6: 15591-15597.

[8] Neiner D, Chiu H W, Kauzlarich S M. Low-temperature solution route to macro scopic amounts of hydrogen terminated silicon nanoparticles[J]. Journal of the American Chemical Society, 2006, 128(34): 11016-11021.

[9] Trill J, Tao C, Winter M, et al. NMR investigations on the lithiation and delithiation of nano silicon-based anodes for Li-ion batteries[J]. Journal of Solid State Electrochemistry, 2011, 15(2): 349-356.

[10] Hwa Y, Kim W S, Yu B C, et al. Facile synthesis of Si nanoparticles using magnesium silicide reduction and its carbon composite as a high-performance anode for Li-ion batteries[J]. Journal of Power Sources, 2014, 252(252): 144-149.

[11] Feng K, Li M, Liu W, et al. Silicon-based anodes for lithium-ion batteries: from fundamentals to practical applications[J]. Small, 2018, 14(8): 1702737.

[12] Liu X H, Wang J W, Huang S, et al. In situ atomic-scale imaging of electrochemical lithiation in silicon[J]. Nature Nanotechnology, 2012, 7(11): 749.

[13] Leung K, Soto F, Hankins K, et al. Stability of solid electrolyte interphase components on lithium metal and reactive anode material surfaces[J]. Journal of Physical Chemistry C, 2016, 120(12):

6302-6313.

[14] Zhang W, Luo G, Xu Q, et al. Enhanced reversible lithium storage for nano-Si with a<10 nm homogeneous porous carbon coating layer[J]. Electrochimica Acta, 2018, 269: 1-10.

[15] Xiao Q, Zhang Q, Fan Y, et al. Soft silicon anodes for lithium ion batteries[J]. Energy & Environmental Science, 2014, 7(7): 2261-2268.

[16] Wu H, Chan G, Choi J W, et al. Stable cycling of double-walled silicon nanotube battery anodes through solid-electrolyte interphase control[J]. Nature Nanotechnology, 2012, 7(5): 310-315.

[17] Li Q, Yu M, Huang Y, et al. Phosphorus-doped silicon copper alloy composites as high-performance anode materials for lithium-ion batteries[J]. Journal of Electroanalytical Chemistry. 2023, 944(117684).

[18] Kim J S, Choi W, Cho K Y, et al. Effect of polyimide binder on electrochemical characteristics of surface-modified silicon anode for lithium ion batteries[J]. Journal of Power Sources, 2013, 244: 521-526.

[19] Ge M, Lu Y, Ercius P, et al. Large-scale fabricaton, 3D tomography, and lithium-ion battery application of porous silicon[J]. Nano Letters, 2013, 14(1): 261-268.

[20] Chai L, Wang X, Bi C, et al. Lifetime optimization of amorphous silicon thin-film anodes for lithium-ion batteries[J]. ACS Applied Energy Materials, 2023

[21] Hui W, Yi C. Designing nanostructured Si anodes for high energy lithium ion batteries[J]. Nano Today, 2012, 7(5): 414-429.

[22] He Z, Liu L, Liu S, et al. A novel design idea of high-stability silicon anodes for lithium-ion batteries: Building in-situ "high-speed channels" while reserving space[J]. Chemical Engineering Journal. 2023, 472(144991).

[23] Wang B, Li W, Wu T, et al. Self-template construction of mesoporous silicon submicrocube anode for advanced lithium ion batteries[J]. Energy Storage Materials, 2018, 15: 139-147.

[24] Wang G Q, Xu B, Shi J, et al. Confined Li ion migration in the silicon-graphene complex system: an ab initio investigation[J]. Applied Surface Science, 2018, 436: 505-510.

[25] BerlaL A, Lee S W, Cui Y, et al. Mechanical behavior of electrochemically lithiated silicon[J]. Journal of Power Sources, 2015, 273: 41-51.

[26] Zhou Y, Guo H, Yong Y, et al. Introducing reduced grapheme oxide to improve the electrochemical performance of silicon-based materials encapsulated by carbonized polydopamine layer for lithium ion batteries[J]. Materials Letters, 2017, 195: 164-167.

[27] Zhou Y, Guo H J, Yan G H, et al. Fluidized bed reaction towards crystalline embedded amorphous Si anode with much enhanced cycling stability[J]. Chemical Communication, 2018, 54(30): 3755-3758.

[28] Roy A K, Zhong M, Schwab M G, et al. Preparation of a binder-free three-dimensional carbon foam/silicon composite as potential material for lithium ion battery anodes[J]. ACS Applied Materials & Interfaces, 2016, 8: 7343-7348.

[29] Fang M, Wang Z, Chen X, et al. Sponge-like reduced graphene oxide/silicon/carbon nanotube composites for lithium ion batteries[J]. Applied Surface Science, 2018, 436: 345-353.

[30] Ye X, Gan C, Huang L, et al. Improving lithium-ion diffusion kinetics in nano-Si@C anode materials with hierarchical MoS2 decoration for high-performance lithium-ion batteries[J]. Chemelectrochem, 2021, 8(7): 1270-1279.

[31] Ma Y, Younesi R, Pan R, et al. Constraining Si particles within graphene foam monolith: Interfacial modification for high-performance Li^+ storage and flexible integrated configuration[J]. Advanced Functional Materials, 2016, 26: 6797-6806.

[32] Kaushik K, Marco-Tulio F R, Stephen E T, et al. Calendar-life versus cycle-life aging of lithium-ion cells with silicon-graphite composite electrodes[J]. Electrochimica Acta, 2018, 280: 221-228.

[33] Li Y, Xu G J, Yao Y F, et al. Improvement of cyclability of silicon-containing carbon nanofiber anodes for lithium-ion batteries by employing succinic anhydride as an electrolyte additive[J]. Journal of Solid State Electrochemistry, 2013, 17(5): 1393-1399.

[34] Jing S L, Jiang H, Hu Y J, et al. Face-to face contact and open-void coinvolved Si/C nanohybrids lithium-ion battery anodes with extremely long cycle life[J]. Advanced Functional Materials, 2015, 25: 5395-5401.

[35] Zhang R, Du Y, Li D, et al. Highly reversible and large lithium storage in mesoporoussi/c nanocomposite anodes with silicon nanoparticles embedded in a carbon framework[J]. Advanced Materials, 2014, 26: 6749-6755.

[36] Zhang X, Qiu X, Kong D, et al. Silicene flowers: A dual stabilized silicon building block for high-performance lithium battery anodes[J]. ACS Nano, 2017, 11(7): 7476-7484.

[37] Li C B, Li T, Kang L, et al. One-step synthesis of hollow structures Si/C composites based on expandable microspheres as anodes for lithium ion batteries[J]. Electrochemistry Communication, 2016, 72: 69-73.

[38] Xu Z L, Zhang B, Kim J K. Electrospun carbon nanofiber anodes containing monodispersed Si and nanoparticles and graphene oxide with exceptional high rate capacities[J]. Nano Energy, 2014, 6: 27-35.

[39] Qi Z Y, Dai L Q, Wang Z F, et al. Optimizing the carbon coating to eliminate electrochemical interface polarization in a high performance silicon anode for use in a lithium-ion battery[J]. New Carbon Materials, 2022, 37(1): 245-258.

[40] Gao P F, Fu J W, Yang J, et al. Microporous carbon coated silicon core/shell nanocomposite via in situ polymerization for advanced Li-ion battery anode material[J]. Physical Chemistry Chemical Physics, 2009, 47(11): 11101-11105.

[41] Yi Z, Lin N, Xu T J, et al. TiO_2 coated Si/C interconnected microsphere with stable framework and interface for high-rate lithium storage[J]. Chemical Engineering Journal, 2018, 347: 214-222.

[42] Cao C T, Iwnetim I A, Eric S, et al. Solid electrolyte interphase on native oxide-terminated silicon anodes for Li-ion batteries[J]. Joule, 2019, 3: 762-781.

[43] Schroder K W, Dylla A G, Harris S J, et al. Role of surface oxides

in the formation of solid-electrolyte interphases at silicon electrodes for lithium-ion batteries[J]. ACS Applied Materials & Interfaces, 2014, 6: 21510-21524.

[44] He W, Tian H J, Xin F X, et al. Scalable fabrication of micro-sized bulk porous Si from Fe-Si alloy as a high performance anode for lithium-ion batteries[J]. Journal of Materials Chemistry A, 2015, 3: 17956-17962.

[45] Zhou X, Yin Y X, Wan L J, et al. Self-assembled nanocomposite of silicon nanoparticles encapsulated in graphene through electrostatic attraction for lithium-ion batteries[J]. Advanced Energy Materials, 2012, 2(9): 1086-1090.

[46] Li Q, Chen D, Li K, et al. Electrostatic self-assembly bmSi@C/rGO composite a anode material for lithium ion battery[J]. Electrochimica Acta, 2016, 202: 140-146.

[47] Du L L, Wei L, Chao L, et al. Lignin derived Si@C composites as a high performance anode material for lithium ion batteries[J]. Solid State Ionics, 2018, 319: 77-82.

[48] Chen Y L, Hu Y, Shen Z, et al. Hollow coreeshell structured silicon@carbon nanoparticles embed in carbon nanofibers as binder-free anodes for lithium-ion batteries[J]. Journal of Power Sources, 2017, 342: 467-475.

[49] Fang S, Shen L F, Xu G Y, et al. Rational design of void-involved Si@TiO_2 nanospheres as high performance anode material for lithium-ion batteries[J]. ACS Applied Materials & Interfaces, 2014, 6: 6497-6503.

[50] Fang S, Tong Z K, Nie P, et al. Raspberry-liked nanostructured silicon composite anode for high performance lithium-ion batteries[J]. ACS Applied Materials & Interfaces, 2017, 9: 18766-18773.

[51] Nie P, Liu X Y, Fu R R, et al. Mesoporous silicon anodes by using polybenzimidazole derived pyrrolic N-enriched carbon toward high-energy Li-ion batteries[J]. ACS Energy letters, 2017, 2: 1279-1287.

[52] Jaumann T, Gerwig M, Balach J, et al. Dichlorosilane-derived nano-silicon inside hollow carbon spheres as a high-performance anode for Li-ion batteries[J]. Journal of Materials Chemistry A, 2017, 5: 9262-9271.

[53] Shi J W, Gao H Y, Hu G X, et al. Core-shell structured Si@C nanocomposite for high-performance Li-ion batteries with a highly viscous gel as precursor[J]. Journal of Power Sources, 2019, 438: 227001.

锂离子电池硅炭负极材料的制备与电化学性能研究

袁立业[1,2,*]，吕春祥[1,2,*]，吕晓轩[1,2]，袁淑霞[1,2]，张　蒽[1,2,3]，曹莉娟[1,2]，杨　禹[1,2]

（1. 中国科学院山西煤炭化学研究所, 碳纤维制备技术国家工程实验室, 山西 太原 030001；
2. 中国科学院山西煤炭化学研究所, 中科院炭材料重点实验室, 山西 太原 030001；
3. 中国科学院大学, 北京 100049）

摘　要： 利用微胶囊技术将酚醛树脂包覆于纳米硅表面，然后在氩气保护下高温炭化，制得硅炭复合负极材料。首先采用 4 种不同质量比的酚醛树脂与纳米硅制备了硅碳复合材料，得到了不同炭质厚度的硅碳复合材料。通过对其循环性能和倍率性能的比较，发现酚醛树脂与纳米硅的质量比为 1∶4，即碳层厚度为 4.5 nm 时，电化学性能最佳。随后对该种硅碳复合材料的综合电化学性能进行了测试，该材料作为负极制备的锂离子电池具有良好的电化学性能，在电流密度为 100 mA g^{-1} 的条件下，其首次放电比容量为 2 382 mAh g^{-1}，首次充电比容量为 1 667 mAh g^{-1}，首次库伦效率为 70%。经 200 次充放电循环后放电比容量为 835.6 mAh g^{-1}，库伦效率为 99.2%。此外，其倍率性能非常优异，在 100、200、500、1 000、2 000 及 100 mA g^{-1} 电流密度下，其平均放电比容量分别为 1 716.4、1 231.6、911.7、676.1、339.8 及 1 326.4 mAh g^{-1}。

关键词： 微胶囊技术；锂离子电池；硅负极；高容量；低成本

中图分类号： 127.1^{+}1　　**文献标识码：** A

通讯作者：袁立业，助理研究员. E-mail: cimigowatano@163.com；
吕春祥，研究员. E-mail: lucx@sxicc.ac.cn

本文的电子版全文由 Elsevier 出版社在 ScienceDirect 上出版（https://www.sciencedirect.com/journal/new-carbon-materials/）